

A Novel Vector-Based Pulse-Width Modulation for Three-Phase Two-Level Voltage Source Inverters

T. Qanbari, B. Tousi ^{*}, M. Farhadi-Kangarlu

Department of Electrical Engineering, Urmia University, Urmia, Iran.

Abstract- The space vector pulse-width modulation (SVPWM) is a simple and suitable method for voltage control of three-phase two-level voltage source inverters (VSIs). However, there are plenty of methods to improve the two-level VSIs performance by adding virtual vectors or sub-sectors to the SVPWM diagram which cause complexity in implementation of SVPWM for VSIs similar to multilevel inverters. Operation in overmodulation mode is the other reason for complexity in conventional SVPWM. This paper proposes a novel modulation method, named as level vector pulse-width modulation (LVPWM), for voltage control of VSIs. The concept of the proposed method is similar to SVPWM but with different vector diagram and dwell times calculations. Unlike the SVPWM, the α and β axes and also their variables are considered separately without gathering in complex variables. The vector diagram has two separated α and β axes each of which contains individual switching vectors and reference vectors. The selection of the vectors to synthesize the reference vectors depends on only the amplitudes of the reference vectors. With lower computational overhead and easy and continuous extension to overmodulation region, the proposed method is a simple solution to the mentioned problems. Simulation and experimental results and harmonics analysis verify the effectiveness of the proposed algorithm.

Keyword: Voltage Source Inverter, Pulse-Width Modulation, Space Vector Modulation, Overmodulation.

1. INTRODUCTION

Two-level voltage source inverter is one of the most common and widely utilized power converter topologies due to its simple structure and reliable operation. Space vector PWM, carrier-based PWM and selective harmonics elimination are the most common methods to voltage control of this inverter [1-3]. SVPWM is the preferred and widely used real-time modulation technique. Easy digital implementation, higher DC voltage utilization, linear voltage gain characteristic, suitability for advanced motor drive systems and improved harmonics content, total harmonics distortion (THD) and common-mode voltage are the advantages of this modulation method [1-7].

SVPWM method for two-level VSIs is a simple to implement algorithm because of easy identification of the reference vector location. However, there are plenty of methods that are proposed to improve the two-level VSI performance by adding virtual vectors or sub-

sectors to the SVPWM diagram. Attractive SVPWM-based torque control schemes to improve the performance of VSI-fed induction motors have been proposed in Refs. [4-6]. These techniques create some virtual vectors in the SVPWM diagram. However, the high number of vectors increases the computational burden of these methods significantly [4]. Four modified SVPWM strategies to reduce the common-mode voltage of VSI have been proposed in Ref. [7]. The sectors of the SVPWM diagram have been divided into different regions in these methods. The current error space vector-based hysteresis controllers for VSI-fed induction motor drives are proposed in Refs. [8, 9]. In these methods also, the SVPWM diagram is divided into sub-sectors. Adaptive neuro-fuzzy inference system based on multi-sector SVPWM scheme for sensor-less brushless DC motor drive has been proposed in Ref. [8]. These recently published research works are samples of the methods which increase the number of vectors or sub-sectors in the SVPWM diagram. Similar to the multilevel inverters, the SVPWM diagram of the VSI with increased vectors or sub-sectors has the problem and complexity of reference vector locating.

Because of the simplicity of the implementation, few researches focus on the reduction of the computational overhead in the SVPWM for two-level VSIs in the

Received: 14 Dec. 2021

Revised: 1 Feb. 2022

Accepted: 5 Feb. 2022

*Corresponding author:

E-mail: b.tousi@urmia.ac.ir (B. Tousi)

DOI: 10.22098/joape.2023.9997.1708

Research Paper

© 2023 University of Mohaghegh Ardabili. All rights reserved.

literature. An efficient method with the construction of a specific intermediate vector using a simple coordinate transformation has been proposed in Ref. [11]. A fast method to compute dwell time values without using either trigonometric functions or even Clarke or Park transformations is presented in Ref. [12]. The hybrid SVPWM strategy proposed in Ref. [13] considers various SVPWM sequences and places the best performance sequence for a given reference vector. A random forest regression-based method with the advantage of rapid implementation and improved prediction for the SVPWM algorithm has been proposed in Ref. [14]. A novel SVPWM using image processing is proposed in Ref. [15]. Space vector diagrams, as well as tip of continuously rotating reference voltage vector, are treated and processed as images. These methods consider operation of the inverter only in normal linear modulation mode.

The other reason for the complexity in SVPWM implementation for VSIs is the overmodulation operation. Generally, VSIs are supplied by grid voltage. A diode-bridge rectifier converts the grid AC voltage to DC voltage. In this condition, the inverter cannot generate the standard voltage of the grid at the border of linear modulation with conventional modulation techniques [16]. Further extension of the output voltage over the linear region can be achieved with overmodulation, which is one of the critical design considerations especially when the inverter is supplied by a diode-bridge rectifier [17, 18]. In the conventional SVPWM method, overmodulation occurs as the reference vector goes beyond the circle inscribed in the hexagon in the vector diagram. However, a distortion of the output voltage occurs and the accurate value of the fundamental component cannot be obtained [17]. Some useful methods have been proposed to improve the VSI performance in the overmodulation region with the SVPWM scheme. An overmodulation strategy for current control in photovoltaic inverters to keep the power generation at low DC-link voltages has been proposed in Ref. [18]. Three optimized PWM techniques for the overmodulation region of two-level inverter-fed AC drives are introduced and investigated from harmonic loss minimization point of view in Ref. [19]. An overmodulation technique is proposed in Ref. [19] based on Fourier analysis. The overmodulation trajectory is a mixture of 6 arc segments of the inscribed circle and 6 vertices of the voltage hexagon in this method. By adjusting the holding angle at each vertex, the modulation index is determined. Complexity and transition from linear to overmodulation region are the

major problems regarding the overmodulation strategies [17]. These methods give no definite relationship between the fundamental component of output voltage and reference voltage and then they are performed through complex real-time calculation or lookup table implementation [19].

This paper proposes a novel modulation method for two-level VSIs similar to the SVPWM concept but with different vector diagram and dwell times calculations to solve the mentioned problems associated with the SVPWM method. In the proposed method, the variables on α and β axes are not gathered in complex variables. The vector diagram has two separated α and β axes each of which contains individual switching vectors and reference vectors. The selection of the vectors to synthesize the reference vectors depends on only the amplitudes of the reference vectors. The proposed method has been applied to a computer-aided simulated and laboratory-built VSI. The effectiveness of the method has been verified by simulation and experimental results and harmonics analysis.

2. LEVEL VECTOR PULSE-WIDTH MODULATION

The circuit diagram of a three-phase two-level VSI is shown in Fig. 1. The sinusoidal references for the phase voltages of the inverter load are as follows:

$$v_{ra}(t) = V_m \sin(\omega t + \varphi) \quad (1)$$

$$v_{rbo}(t) = V_m \sin(\omega t - \frac{2\pi}{3} + \varphi) \quad (2)$$

$$v_{rco}(t) = V_m \sin(\omega t + \frac{2\pi}{3} + \varphi). \quad (3)$$

where V_m is the amplitude, ω is the angular velocity and φ is the phase delay angle. It is possible to transform these voltage references to equivalent two-phase variables using Clarke transformation [1]:

$$\begin{bmatrix} V_{ra}(t) \\ V_{r\beta}(t) \end{bmatrix} = \frac{2}{3} \begin{bmatrix} 1 & -\frac{1}{2} & -\frac{1}{2} \\ 0 & \frac{\sqrt{3}}{2} & -\frac{\sqrt{3}}{2} \end{bmatrix} \begin{bmatrix} v_{ra}(t) \\ v_{rbo}(t) \\ v_{rco}(t) \end{bmatrix}. \quad (4)$$

According to this transformation, V_{ra} and $V_{r\beta}$ are

$$V_{ra}(t) = \frac{2}{3} (v_{ra}(t) - \frac{1}{2} (v_{rbo}(t) + v_{rco}(t))) = V_m \sin(\omega t + \varphi) \quad (5)$$

$$V_{r\beta}(t) = \frac{\sqrt{3}}{3} (v_{rbo}(t) - v_{rco}(t)) = -V_m \cos(\omega t + \varphi) \quad (6)$$

Using this transformation, the inverter has two voltage references. In conventional SVPWM, after transferring the three-phase variables to equivalent two-phase variables, the variables are considered in complex coordinate (α - β coordinate). This is the first and main reason for the complexity in the implementation of SVPWM. Of course, as mentioned, the conventional

SVPWM is a simple and suitable method for voltage control of VSIs. However, there are plenty of methods to improve the two-level VSI performance by adding virtual vectors or sub-sectors to the SVPWM diagram which cause complexity in the implementation of SVPWM for VSIs similar to multilevel inverters. Operation in overmodulation mode is the other reason for complexity in conventional SVPWM. In the proposed method, both of the variables (α and β) are considered as real (not imaginary) variables on two separated axes without gathering in complex variables.

There are eight possible combinations of switching states in the VSI. The switching states, the corresponding load voltages and the Clarke transformations of these voltages are listed in Table 1. Switching state '1' denotes that the upper switch in the inverter leg is on and switching state '0' denotes that this switch is off. Fig. 2 shows the transferred values of the voltage references (V_{ra} and $V_{r\beta}$) and also the transferred values of the output voltages of the inverter (V_α and V_β) for each switching state. As listed in Table 1 and shown in Fig. 2, V_α and V_β are defined by vectors ($V_{\alpha 1}$ to $V_{\alpha 7}$ and $V_{\beta 1}$ to $V_{\beta 7}$) for each switching state. Each vector represents a level in the V_α and V_β waveform. Hence, these vectors are named level vectors. The switching states [000] and [111] have equal values of V_α and V_β . In other words, $V_{\alpha 1}$ and $V_{\beta 1}$ have two switching states, one of which is redundant. Each of the sinusoidal voltage references also can be modeled by a vector. Fig. 3 shows the level vectors and the reference vectors on the α and β axes. This figure is the vector diagram of the proposed modulation method. This vector diagram has two separated α and β axes each of which contains individual switching vectors and reference vectors. The level vectors are fixed and the amplitudes of the reference vectors vary sinusoidally. The selection of the vectors to synthesize the reference vectors depends on only the amplitudes of the reference vectors. In order to produce the desired output voltage, the inverter must synthesize the reference vectors by the level vectors at each sampling period by proper selection of the switching states.

Table 1. The switching states, the corresponding load voltages and Clarke transformation of these voltages

Switching States	v_a	v_b	v_c	V_α	V_β
(000)	0	0	0	0 ($V_{\alpha 1}$)	0 ($V_{\beta 1}$)
(001)	$-V_d/3$	$-V_d/3$	$2V_d/3$	$-V_d/3$ ($V_{\alpha 2}$)	$-\sqrt{3}V_d/3$ ($V_{\beta 2}$)
(010)	$-V_d/3$	$2V_d/3$	$-V_d/3$	$-V_d/3$ ($V_{\alpha 3}$)	$\sqrt{3}V_d/3$ ($V_{\beta 3}$)
(011)	$-2V_d/3$	$V_d/3$	$V_d/3$	$-2V_d/3$ ($V_{\alpha 4}$)	0 ($V_{\beta 4}$)
(100)	$2V_d/3$	$-V_d/3$	$-V_d/3$	$2V_d/3$ ($V_{\alpha 5}$)	0 ($V_{\beta 5}$)
(101)	$V_d/3$	$-2V_d/3$	$V_d/3$	$V_d/3$ ($V_{\alpha 6}$)	$-\sqrt{3}V_d/3$ ($V_{\beta 6}$)
(110)	$V_d/3$	$V_d/3$	$-2V_d/3$	$V_d/3$ ($V_{\alpha 7}$)	$\sqrt{3}V_d/3$ ($V_{\beta 7}$)
(111)	0	0	0	0 ($V_{\alpha 1}$)	0 ($V_{\beta 1}$)

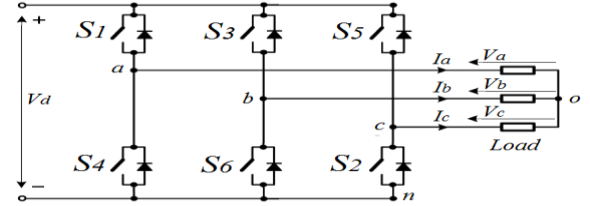


Fig. 1. Circuit diagram of the three-phase two-level VSI

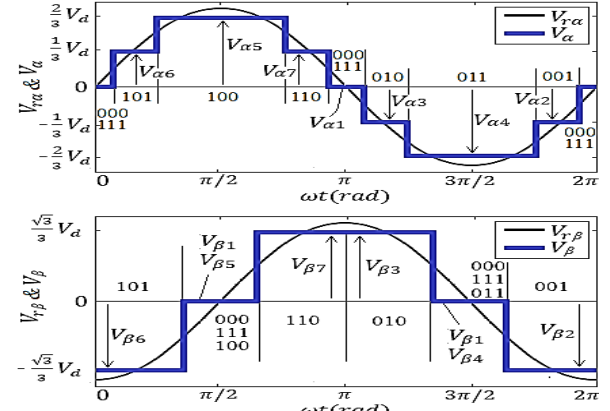


Fig. 2. The transferred values of the voltage references and the output voltages of the inverter for each switching state

Similar to the SVPWM, three nearby level vectors synthesize the reference vectors during a sampling period (T_s) in the proposed modulation method. As an example, Fig. 4 shows the synthesis of V_α by $V_{\alpha 1}$, $V_{\alpha 2}$ and $V_{\alpha 6}$ and the synthesis of V_β by $V_{\beta 1}$, $V_{\beta 2}$ and $V_{\beta 6}$. Each switching state has a dwell time in the sampling period. The dwell times values must be calculated such that the integral of V_α be equal to integral of V_{ra} and also the integral of V_β be equal to integral of $V_{r\beta}$ in the sampling period as follows:

$$A_{\alpha 1} + A_{\alpha 2} + A_{\alpha 3} = A_{\alpha r}, \quad (7)$$

$$A_{\beta 1} + A_{\beta 2} + A_{\beta 3} = A_{\beta r}, \quad (8)$$

where $A_{\alpha 1}$, $A_{\alpha 2}$ and $A_{\alpha 3}$ are the areas of V_α for each of the three selected switching states, $A_{\beta 1}$, $A_{\beta 2}$ and $A_{\beta 3}$ are the areas of V_β for each of the three selected switching states and $A_{\alpha r}$ and $A_{\beta r}$ are the areas V_{ra} and $V_{r\beta}$ in the sampling period. $A_{\alpha r}$ and $A_{\beta r}$ can be calculated as follows:

$$A_{\alpha r} = I_{\alpha r} = \int_{t_0}^{t_0+T_s} V_{\alpha r} dt = \frac{V_m}{\omega} [\cos(\omega t_0 + \varphi) - \cos(\omega t_0 + \omega T_s + \varphi)] \quad (9)$$

$$A_{\beta r} = I_{\beta r} = \int_{t_0}^{t_0+T_s} V_{\beta r} dt = \frac{V_m}{\omega} [\sin(\omega t_0 + \varphi) - \sin(\omega t_0 + \omega T_s + \varphi)] \quad (10)$$

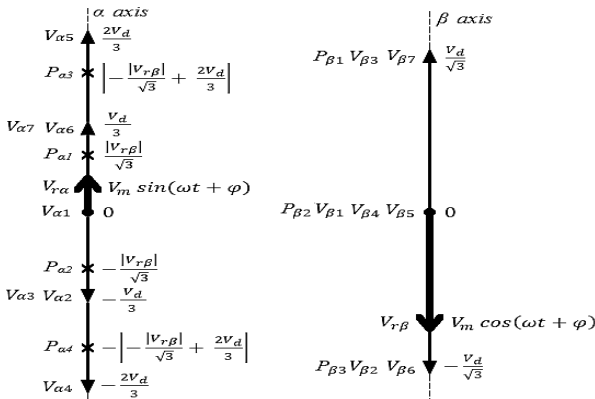
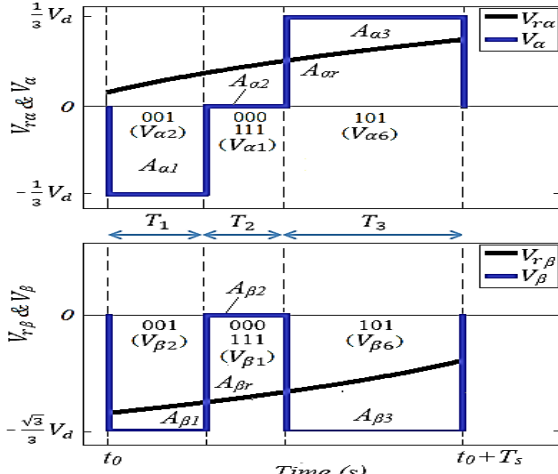
$$\frac{V_m}{\omega} [\sin(\omega t_0 + \varphi) - \sin(\omega t_0 + \omega T_s + \varphi)]$$

where t_0 is the starting point of each sampling period. Then, the following system of equations gives the dwell times values of the selected vectors:

$$\begin{cases} V_{\alpha 1} T_1 + V_{\alpha 2} T_2 + V_{\alpha 3} T_3 = I_{\alpha r} \\ V_{\beta 1} T_1 + V_{\beta 2} T_2 + V_{\beta 3} T_3 = I_{\beta r} \\ T_1 + T_2 + T_3 = T_s \end{cases} \quad (11)$$

Table 2. The regions on the axes and the admissible level vectors to synthesize the reference vectors

Region on α Axis	Admissible Vectors to Synthesize $V_{\alpha r}$	Region on β Axis	Admissible Vectors to Synthesize $V_{\beta r}$
$P_{\alpha 2} \leq V_{ra} \leq P_{\alpha 1}$	$V_{a1}, V_{a2}, V_{a3}, V_{a6}$ V_{a7}	$P_{\beta 2} \leq V_{r\beta} \leq P_{\beta 1}$	$V_{\beta 1}, V_{\beta 3}, V_{\beta 4}, V_{\beta 5}$ $V_{\beta 7}$
$P_{\alpha 1} \leq V_{ra} \leq P_{\alpha 3}$	$V_{a1}, V_{a5}, V_{a6}, V_{a7}$	$P_{\beta 3} \leq V_{r\beta} \leq P_{\beta 2}$	$V_{\beta 1}, V_{\beta 2}, V_{\beta 4}, V_{\beta 5}$ $V_{\beta 6}$
$P_{\alpha 4} \leq V_{ra} \leq P_{\alpha 2}$	$V_{a1}, V_{a2}, V_{a3}, V_{a4}$		

**Fig. 3. The vector diagram of the proposed modulation method****Fig. 4. Synthesis of $V_{\alpha r}$ and $V_{\beta r}$ by V_{α} and V_{β} in one sampling period**

In Eq. 11, V_{sa1} , V_{sa2} and V_{sa3} are the three selected vectors from α axis, V_{sb1} , V_{sb2} and V_{sb3} are the three selected vectors from β axis and T_1 , T_2 and T_3 are the dwell times of the corresponding switching states of these vectors in the sampling period respectively. V_{sa1} , V_{sa2} and V_{sa3} have common switching states with V_{sb1} , V_{sb2} and V_{sb3} respectively. Obviously, the dwell times values must be positive. So, the above system of equations specifies which of the level vectors must be selected to synthesize the reference vectors. The selection of the proper level vectors at each sampling period depends on the locations of the reference vectors. Solving (11) denotes that each group of the level vectors

has positive dwell time values for definite and limited values of the reference vectors. The points $P_{\alpha 1}$, $P_{\alpha 2}$, $P_{\alpha 3}$ and $P_{\alpha 4}$ divide the α axis into five regions and the points $P_{\beta 1}$, $P_{\beta 2}$ and $P_{\beta 3}$ divide the β axis into four regions. These points have the following values:

$$P_{\alpha 1} = -P_{\alpha 2} = \frac{|V_{r\beta}|}{\sqrt{3}}, \quad (12)$$

$$P_{\alpha 3} = -P_{\alpha 4} = \left| -\frac{|V_{r\beta}|}{\sqrt{3}} + \frac{2V_d}{3} \right|, \quad (13)$$

$$P_{\beta 1} = -P_{\beta 3} = \frac{V_d}{\sqrt{3}}, \quad (14)$$

$$P_{\beta 2} = 0. \quad (15)$$

In each region between these points, there is a group of the level vectors that satisfy Eq. (11) to synthesize the reference vectors. Depending on the values and locations of the reference vectors, the admissible level vectors to be selected to synthesize the reference vectors are listed in Table 2. Between the admissible level vectors, the vectors with common switching states are the selected vectors to synthesize the reference vectors in each sampling period. For example, at the locations of the reference vectors in Fig. 3, the vectors V_{a1} , V_{a2} , V_{a3} , V_{a6} and V_{a7} are the admissible vectors to synthesize V_{ra} and the vectors $V_{\beta 1}$, $V_{\beta 2}$, $V_{\beta 4}$, $V_{\beta 5}$ and $V_{\beta 7}$ are the admissible vectors to synthesize $V_{r\beta}$. Between these vectors, V_{a1} with $V_{\beta 1}$, V_{a2} with $V_{\beta 2}$ and V_{a6} with $V_{\beta 6}$ have the common switching states. Then, these vectors are the proper vectors to synthesize the reference vectors at these points. Fig. 5 shows a sample of the V_{α} and V_{β} waveforms synthesized by the proposed method in one cycle.

According to Eqns. (12) to (15), the maximum value for both of V_{ra} and $V_{r\beta}$ to satisfy the system of equations (11) is $\sqrt{3}V_d/3$. For higher values, the system of equations gives negative values for dwell times. Then, the amplitudes of the voltage references in modulation region, can vary from $-\sqrt{3}V_d/3$ to $\sqrt{3}V_d/3$ as follows:

$$V_m = m \frac{\sqrt{3}}{3} V_d, \quad 0 \leq m \leq 1 \quad (16)$$

where m is the modulation index.

After selecting the level vectors and calculating their dwell times, switching sequence arranging is the next step. The aim of a proper switching sequence design is to minimize the switching frequencies of the devices. Fig. 6 shows the seven-segment switching sequences in the proposed modulation for two different positions of the reference vectors. At each transition from one switching state to the next, only one switch turns on and one switch turns off. The redundant switching states of V_{a1} and $V_{\beta 1}$ (000 and 111) are utilized to reduce the

number of switchings. Each of the switches in the inverter is turned on and off once per sampling period. So the switching frequency of the devices is equal to the sampling frequency. Unlike the hexagonal space vector diagram, the level vector diagram has a simple linear topology such that identification of the reference vectors locations to select the proper switching states is simple with any number of vectors. Moreover, the reference vector is considered constant during T_s in SVPWM methods [1]. This consideration causes an error in the synthesis of the reference vector, particularly with low sampling frequencies. According to equations (7) to (11), the proposed method considers accurate values of the reference vectors in each sampling time and then the inverter can produce output voltage with fundamental component exactly equal to the reference value and improved harmonics content and THD.

As discussed, similar to the conventional SVPWM, the switching frequency of the devices is equal to the sampling frequency. Switching losses is the main factor in the efficiency of converters and it is dependent on the switching frequency. So, the efficiency of a VSI controlled by the proposed method is equal to the efficiency of that VSI controlled by conventional SVPWM with equal sampling frequencies. As mentioned, there are plenty of methods that are proposed to improve the two-level VSI performance by adding virtual vectors or sub-sectors to the SVPWM diagram. These methods have problems of the complexity similar to SVPWM for multilevel inverters.

Table 3. The regions and the admissible vectors to synthesize the reference vectors in overmodulation mode

Region on α Axis	Admissible Vectors to Synthesize $V_{\alpha r}$	Region on β Axis	Admissible Vectors to Synthesize $V_{\beta r}$
$V_{\alpha r} > P_{\alpha 3}$	V_{a5}, V_{a6}, V_{a7}	$V_{\beta r} > P_{\beta 1}$	$V_{\beta 3}, V_{\beta 7}$
$V_{\alpha r} < P_{\alpha 4}$	V_{a2}, V_{a3}, V_{a4}	$V_{\beta r} < P_{\beta 3}$	$V_{\beta 2}, V_{\beta 6}$

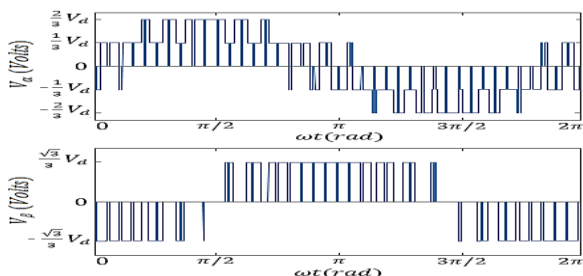


Fig. 5. V_α and V_β waveforms synthesized by the proposed method in one cycle

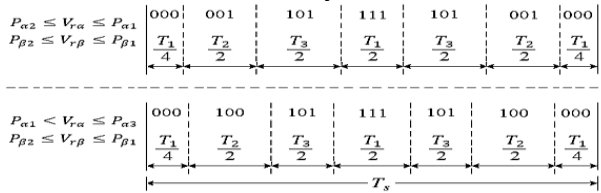


Fig. 6. The seven-segment switching sequences in the proposed modulation for two different positions of the reference vectors

With the lower computational overhead, the proposed method is a simple solution to these problems. The virtual vectors can be easily added to the vector diagram. Instead of sub-sectors, both of the axes in the vector diagram can be divided into various regions.

3. OVERMODULATION

Similar to the conventional SVPWM method, there is a linear relationship between the output voltage and the input DC voltage in the range of $0 \leq m \leq 1$ in the proposed method. According to (16), the maximum value of the fundamental line to line output voltage RMS is equal to $0.707V_d$. In order to produce output voltage with higher values, the inverter operation extends to overmodulation. For m values higher than 1, the reference vectors may lie in regions out of the modulation regions of the proposed method diagram (Fig. 3 and Table 2) in some time intervals. These regions are overmodulation regions. When at least one of the reference vectors lies in overmodulation regions of the diagram, they cannot be synthesized by three level vectors. In other words, there is not any group of level vectors to satisfy Eq. (11). So, only one of the level vectors which is the closest vector to the reference vectors in each axis is the admissible vector to be selected. The admissible level vectors to synthesize the reference vectors in these regions are listed in Table 3. The principle of the proposed method for overmodulation operation is similar to the presented linear modulation operation. Depending on the reference vectors locations, the number of the admissible level vectors with common switching states maybe three or one. Then, the proposed method has two strategies for overmodulation mode:

- 1) If both of the reference vectors lie in the linear modulation region, operates similar to the linear modulation operation. Selection of three level vectors and computation of the dwell times according to Eq. (11).
- 2) If at least one of the reference vectors lies in the overmodulation region, selects only one level vector in the sampling time period.

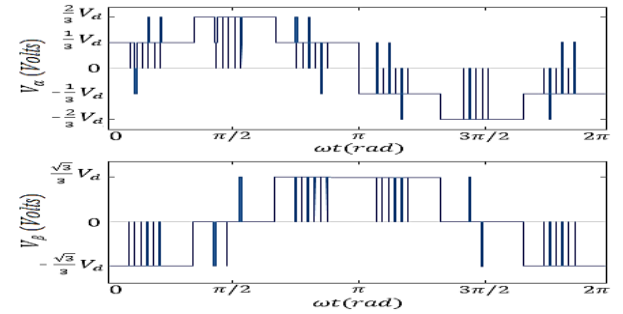


Fig. 7. V_α and V_β waveforms synthesized by the proposed method in overmodulation mode

Fig. 7 shows a sample of the V_α and V_β waveforms in the overmodulation mode. Fig. 8 shows a sample of the V_α and V_β waveforms and V_{ra} and V_{rb} locations in overmodulation mode in the first quarter of one cycle ($0 \leq \omega t \leq \pi/2$). The fundamental component of the phase a voltage of the load can be expressed using Fourier decomposition as follows:

$$\begin{aligned} V_{a1} = & \frac{1}{\pi} \int_0^{2\pi} V_a(\omega t) \sin(\omega t) d\omega t = \\ & \left[\frac{4}{\pi} \int_{\theta_1}^{\theta_3} V_d \sin(\omega t) d\omega t + \frac{4}{\pi} \int_{\theta_5}^{\theta_2} V_d \sin(\omega t) d\omega t \right] + \\ & \left[\frac{4}{\pi} \int_0^{\theta_1} \frac{1}{3} V_d \sin(\omega t) d\omega t + \frac{4}{\pi} \int_{\theta_3}^{\theta_4} \frac{1}{3} V_d \sin(\omega t) d\omega t + \right. \\ & \left. \frac{4}{\pi} \int_{\theta_4}^{\theta_5} \frac{2}{3} V_d \sin(\omega t) d\omega t \right] = \\ & \left[\frac{2mV_d}{\pi\sqrt{3}} \left(\frac{\pi}{2} - \theta_1 + \theta_3 - \theta_5 \sin \theta_1 \cos \theta_1 - \sin \theta_3 \cos \theta_3 \right. \right. \\ & \left. \left. + \sin \theta_5 \cos \theta_5 \right) \right] + \left[\frac{4V_d}{3\pi} (1 - \cos \theta_1 + \cos \theta_3 + \cos \theta_4 - 2 \cos \theta_5) \right]. \end{aligned} \quad (17)$$

The θ angles correspond to the confluences of the reference vectors and the points P on the α and β axes. At θ_1 , V_{rb} enters in the modulation region and is equal to $P_{\beta 3}$:

$$\left| m \frac{\sqrt{3}}{3} V_d \cos \theta_1 \right| = \left| -\frac{\sqrt{3}}{3} V_d \right|, \quad (18)$$

$$\cos \theta_1 = \frac{1}{m}. \quad (19)$$

Similarly, values of other angles can be calculated.

$$\theta_2 = \frac{\pi}{6}, \quad (20)$$

$$\sin(\theta_3 + \frac{\pi}{6}) = \frac{1}{m}, \quad (21)$$

$$\theta_4 = \frac{\pi}{3}, \quad (22)$$

$$\cos(\theta_5 - \frac{\pi}{6}) = \frac{1}{m}. \quad (23)$$

Substituting Eqns. (19) to (23) into Eq. (17) gives the relationship of V_{a1} and m in overmodulation mode:

$$V_{a1} = \frac{2V_d}{\pi} \left[\sqrt{3} \left(\frac{\pi}{6} - \arccos \left(\frac{1}{m} \right) \right) m + \frac{\sqrt{3m^2 - 3} - 1}{m} + 1 \right]. \quad (24)$$

Substituting Eq. (16) into the above equation and a third-order approximation gives the relationship of V_m and V_{a1} :

$$V_m = \frac{\sqrt{3}}{3} V_d \left[\left(\sqrt{\Delta} - \frac{q}{2} \right)^{\frac{1}{3}} - \left(\sqrt{\Delta} + \frac{q}{2} \right)^{\frac{1}{3}} - \frac{a}{3} \right], \quad (25)$$

$$\Delta = \frac{q^2}{4} + \frac{p^3}{27}, \quad (26)$$

$$q = \frac{2a^3}{27} - \frac{ab}{3} + c, \quad (27)$$

$$c = -0.1023 \left(\frac{V_{a1}}{V_d} \right) - 1.5717.$$

(28)

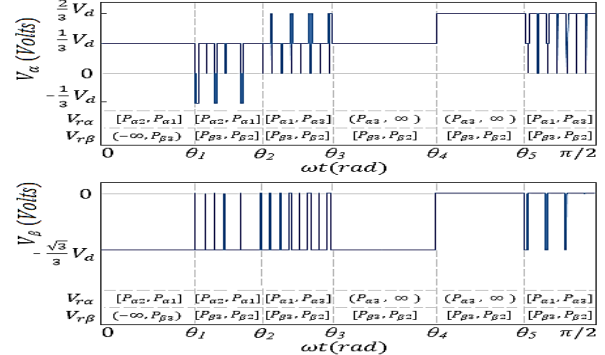


Fig. 8. V_α and V_β waveforms and V_{ra} and V_{rb} locations in overmodulation mode in the interval ($0 \leq \omega t \leq \pi/2$)

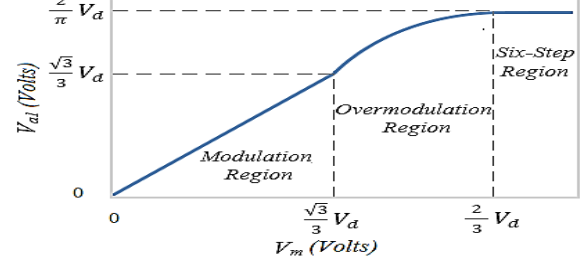


Fig. 9. V_{a1} versus V_m in the modulation, overmodulation and six-step modes

where a , b and p are -3.5335 , 4.1643 and 0.0026 respectively. These coefficients are independent of m , V_{a1} , V_m and V_d values. Fig. 9 shows V_{a1} versus V_m in the linear modulation, the overmodulation and six-step modes. For $V_m \geq 2V_d/3$, there is at least one reference vector that lies in the overmodulation region at each time and the inverter enters in six-step mode and then V_{a1} has constant value equal to $2V_d/\pi$ in this condition. Then the maximum value of the fundamental line to line output voltage RMS can be increased up to $0.78V_d$.

4. HARMONICS ANALYSIS

The line a to line b output voltage of the inverter ($V_{ab}(t)$) can be expressed using Fourier decomposition as follows:

$$V_{ab}(t) = \sum_{n=1}^{\infty} V_{abn} \sin(n\omega t), \quad (29)$$

$$V_{abn} = \frac{1}{\pi} \int_0^{2\pi} V_{ab}(\omega t) \sin(n\omega t) d\omega t. \quad (30)$$

The integral interval in Eq. (30) must be divided into sampling times of the modulation method.

$$\begin{aligned} V_{abn} = & \frac{1}{\pi} \left[\int_0^{t_{s1}} V_{ab}(\omega t) \sin(n\omega t) d\omega t + \right. \\ & \left. \int_{t_{s1}}^{t_{s2}} V_{ab}(\omega t) \sin(n\omega t) d\omega t + \dots \right] \quad (31) \end{aligned}$$

$$\begin{aligned} & + \int_{t_{s(k-1)}}^{2\pi} V_{ab}(\omega t) \sin(n\omega t) d\omega t \\ & = \frac{1}{\pi} \sum_{i=1}^k \int_{t_{s(i-1)}}^{t_{si}} V_{ab}(\omega t) \sin(n\omega t) d\omega t, \end{aligned}$$

$$k = \frac{f_s}{f_o}, \quad (32)$$

$$t_{si} - t_{s(i-1)} = T_s. \quad (33)$$

where f_o and f_s are the fundamental and sampling frequencies. On the other hand, each sampling time is divided to seven segments. Therefore:

$$\begin{aligned} V_{abn} = & \frac{2}{\pi} \sum_{i=1}^k \left[\int_{t_{s(i-1)}}^{t_1} V_{ab}(\omega t) \sin(n\omega t) d\omega t + \right. \\ & \int_{t_1}^{t_2} V_{ab}(\omega t) \sin(n\omega t) d\omega t + \\ & \int_{t_2}^{t_3} V_{ab}(\omega t) \sin(n\omega t) d\omega t \\ & \left. + \int_{t_3}^{t_4} V_{ab}(\omega t) \sin(n\omega t) d\omega t, \right] \end{aligned} \quad (34)$$

where $t_1 = t_{s(i-1)} + T_1/4$, $t_2 = t_1 + T_2/2$, $t_3 = t_2 + T_3/2$ and $t_4 = t_3 + T_4/4$. The above equation determines amplitudes of the harmonic components of the line to line output voltage. By determination of the harmonics content, the THD of V_{ab} can also be calculated. Fig. 10, Fig. 11 and Fig. 12 compare the harmonic spectrums, THD values and common-mode voltages of the inverter controlled by SVPWM and LVPWM methods with the same conditions ($f_o = 50$ Hz, $f_s = 3$ kHz) respectively. Compared with the SVPWM method, the proposed LVPWM method presents slightly improved harmonic spectrum, THD and common mode voltage. This is because of accurate synthesizing of reference vectors.

5. IMPLEMENTATION

The proposed LVPWM method is a real-time modulation technique with easy digital implementation. Implementation of this method has the following steps:

1) Receiving amplitude (V_{al}), frequency (f_o) and angle (φ) of the fundamental component of the phase voltage as the reference signals.

2) Calculating amplitudes of the voltage references:

$$V_m = \begin{cases} V_{al}, & V_{al} \leq \frac{\sqrt{3}}{3} V_d \\ \text{Equation(25)}, & V_{al} \geq \frac{\sqrt{3}}{3} V_d \end{cases}. \quad (35)$$

3) Selecting proper level vectors to synthesize the reference vectors according to Table 2 and Table 3 at each sampling time.

4) Computing dwell times values from Eq. (11) if three level vectors are selected at each sampling time. Permanently at each sampling time, $V_{\alpha l}$ and $V_{\beta l}$ are one of the three selected level vectors on each axis in the linear modulation region. So, the three-by-three system of equation can be simplified as follows:

$$\begin{cases} V_{sa2} T_2 + V_{sa3} T_3 = I_{\alpha r} \\ V_{s\beta 2} T_2 + V_{s\beta 3} T_3 = I_{\beta r} \end{cases}. \quad (36)$$

Then

$$T_2 = \frac{V_{s\beta 3} I_{\alpha r} - V_{sa3} I_{\beta r}}{V_{sa2} V_{s\beta 3} - V_{sa3} V_{s\beta 2}}, \quad (37)$$

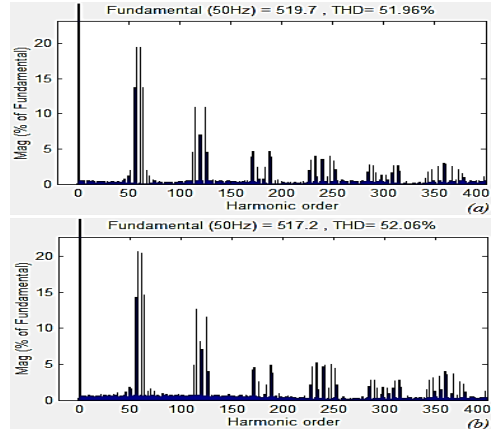


Fig. 10. Line voltage harmonic spectrums with (a) LVPWM method and (b) SVPWM method for $m=1$

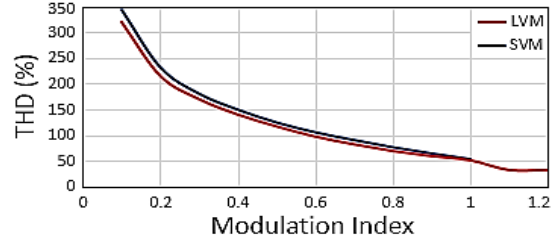


Fig. 11. Line voltage THD values in terms of the modulation index with LVPWM and SVPWM methods

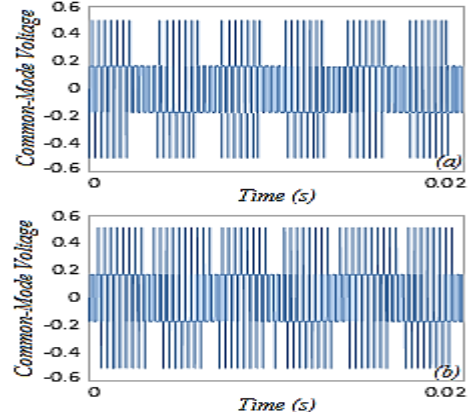


Fig. 12. Normalized common-mode voltages of the inverter with (a) LVPWM method and (b) SVPWM method for $m=1$

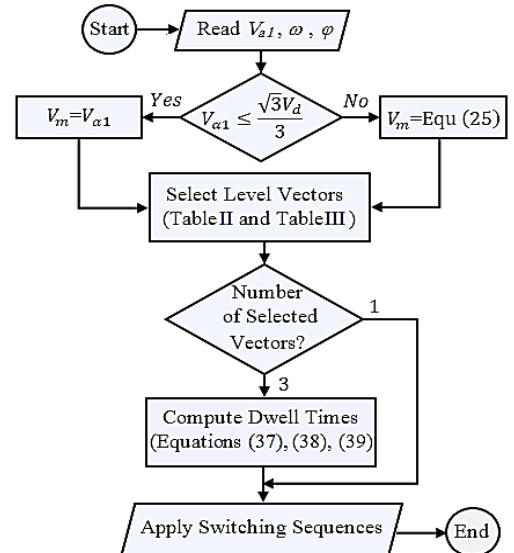


Fig. 13. Flowchart of the proposed algorithm

$$T_3 = \frac{V_{sa2} I_{\beta r} - V_{s\beta 2} I_{ar}}{V_{sa2} V_{s\beta 3} - V_{sa3} V_{s\beta 2}}, \quad (38)$$

$$T_1 = T_s - T_2 - T_3. \quad (39)$$

5) Producing gate signals with switching sequence design considerations at each sampling time.

The flowchart of the proposed algorithm is shown in Fig. 13.

6. FEATURES AND COMPARISONS

The proposed LVPWM method is a different way of implementing SVPWM. As discussed, the VSI has similar characteristics with both the SVPWM and LVPWM. DC voltage utilization, switching frequency, harmonics components, THD and common-mode voltage of the inverter are almost equal with both of the methods. Nevertheless, the proposed LVPWM has the following advantages compared with the SVPWM-based methods [1], [11-15]:

1. The computational overhead of the conventional SVPWM and the proposed LVPWM in normal conditions and linear modulation mode are almost equal. Both of the methods have simple algorithms using simple lookup tables. The proposed method has no considerable advantages compared with the conventional and simplified SVPWMs in these conditions. However, as mentioned, there are plenty of methods to improve the two-level VSI performance by adding virtual vectors or sub-sectors to the SVPWM diagram which cause complexity in the implementation of SVPWM for VSIs similar to multilevel inverters. In these cases, the SVPWM must be implemented analytically without lookup tables. An example is the discrete space vector modulation based on the predictive torque control scheme which improves the performance of a VSI-fed induction motor drive [4], [20]. In this method, besides 8 real space vectors, 30 virtual vectors are considered to avoid high torque ripples and stator current harmonics. Fig. 14(a) shows the space vector diagram of the VSI containing 8 real vectors and 30 virtual vectors. The reference vector locating and implementation of this method has a complex process

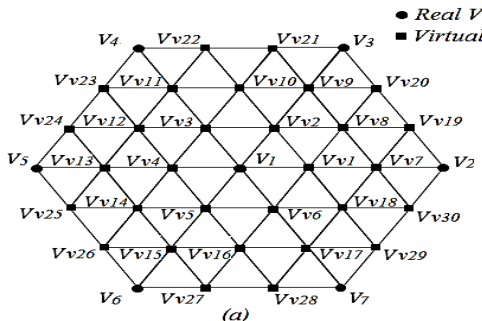
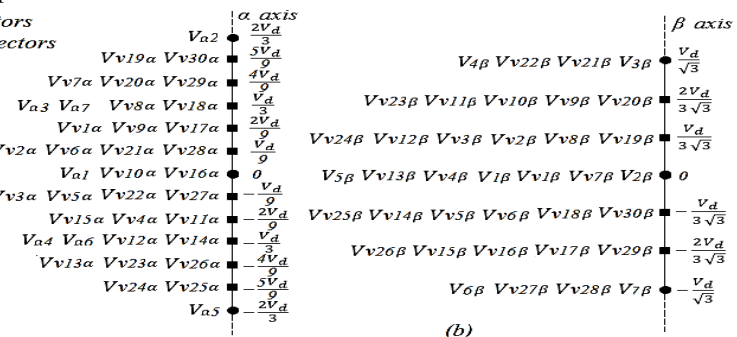


Fig. 14. Predictive torque control scheme with additional virtual vectors: (a) space vector diagram, (b) level vector diagram

similar to the SVPWM for multilevel inverters [4], [20]. In other words, the simple space vector diagram of the VSI has been changed to a complex diagram. Fig. 14(b) shows the proposed level vector diagram considering the predictive torque control scheme. Similar to the space vector diagram, 30 virtual level vectors have been added to this diagram. With any number of vectors, locating the level vectors in this diagram is simple as well as the basic diagram (Fig. 3). Another example is the reduction of the VSI common-mode voltage using the model predictive control strategy [21]. In this strategy, the space vector diagram is divided into different regions with the virtual vectors and inner hexagon that make locating the reference vector difficult as shown in Fig. 15(a). The level vector diagram of the proposed method considering the model predictive control strategy for common-mode voltage reduction is shown in Fig. 15(b). The LVPWM diagram can be divided into any number of regions considering any number of virtual vectors without any complexity in operation.

2. The conventional and simplified SVPWM methods consider the operation of the inverter in only linear modulation mode. For operation in overmodulation mode, there are some independent methods and solutions. Therefore, the operation of a VSI in both the linear modulation and overmodulation modes requires two independent methods. These methods are inherently more complicated than the methods of operation in linear modulation mode. While the proposed method conveniently selects the switching vectors in the overmodulation condition and hence results in a smooth transition from linear to overmodulation region without requiring complex computations or lookup tables. The relationship between the reference vector and the fundamental component of the output voltage in overmodulation mode has been simply determined. The previous overmodulation methods use complex calculations or lookup tables [16-19]. Fig. 16 shows the space vector diagram of the sector-based overmodulation method proposed in Ref. [19].



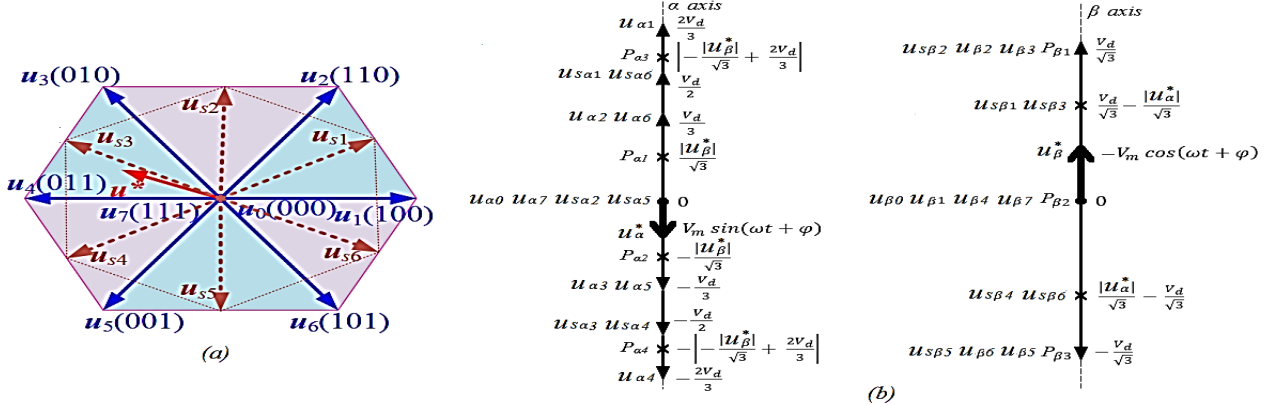


Fig. 15. Model predictive control strategy for common-mode voltage reduction with additional virtual vectors: (a) space vector diagram, (b) level vector diagram

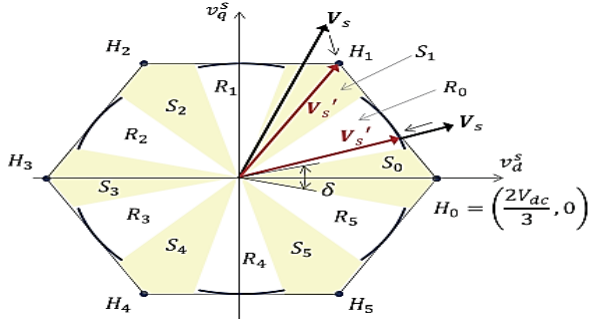


Fig. 16. Space vector diagram of the sector-based overmodulation method proposed in Ref. [19]

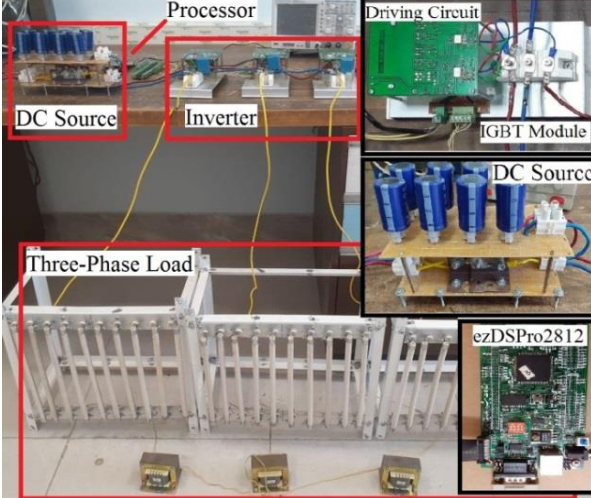


Fig. 17. Experimental setup

In this method, the six phase angles of the reference vector in which the reference vector goes beyond the hexagon are calculated. Out of the hexagon, the nearest space vector is selected. This method is simple and attractive. However, the proposed LVPWM has lower computational burden and memory requirements.

In summary, the proposed LVPWM is a simple method for voltage control of VSIs which covers the operation of the inverter in normal linear modulation mode, operation with methods with additional virtual vectors and also the operation of the inverter in overmodulation mode.

Table 4. Characteristics of the prototype

Item	Value
Output voltage (L-L RMS, f_o)	0-410 V, (1-150 Hz)
Sampling frequency	3 kHz
Input DC voltage	525 V
Load	$R=10\Omega$, $L=21mH$
Rated Power	S=15 kVA
The switches characteristics	IGBT, 1200V, 75A

7. SIMULATION AND EXPERIMENTAL RESULTS

A three-phase two-level 15-kVA VSI with the characteristics given in table 4 and controlled by the proposed LVPWM method is simulated and implemented. The simulations are performed using Matlab/Simulink. Fig. 17 shows a picture of the prototype. The DC source has been provided by a three-phase diode-bridge rectifier. The semiconductor switches are the half-bridge IGBT modules (LS LUH75G1202). The LVPWM technique has been implemented by ezDSPro F2812 board (TMS320F2812). The sampling frequency is 3 kHz. The required drive board is designed using HCPL-316J which is a fast and intelligent IGBT driver. The inverter supplies a laboratory-built three-phase resistive-inductive load (heating elements ($R=10\Omega$) and inductors ($L=21mH$)).

The three-phase diode-bridge rectifier converts the grid 380V AC voltage to DC voltage. Then, the average value of the input DC voltage of the inverter is roughly equal to 525V in this system. Fig. 18 shows the input DC voltage waveform. With this input voltage, the inverter must operate in overmodulation region in order to generate the standard 380V voltage with conventional modulation techniques [13] and also with the proposed LVPWM method. Fig. 19 shows the simulated switching pulses and corresponding phase voltages of the VSI for linear modulation ($m=0.96$) and overmodulation conditions ($m=1.07$) in one cycle. Fig. 20 shows the experimental phase voltages of the

inverter and the phase voltages and currents of the load in standard conditions (220V RMS) in which the inverter operates in the overmodulation region. Fig. 21 shows the simulated and experimental line voltages, phase voltages and currents of the load in three different conditions. Firstly, the reference signals V_{al} , f_0 and φ are 184 Volts, 33 Hertz and 0 degrees respectively and the inverter operates in the linear modulation region. Then the inverter output transfers to the point $V_{al}=224$, $f_0=84$ and $\varphi=42^\circ$, operating in the overmodulation region. Finally, the inverter operation passes to six-step mode ($V_{al}=236$, $f_0=142$ and $\varphi=15^\circ$). This figure shows the easy and continuous extension of the inverter operation to the overmodulation region with the proposed LVPWM method. The simulation and experimental results demonstrate the valid performance of the proposed modulation method and continuous extension to the overmodulation region.

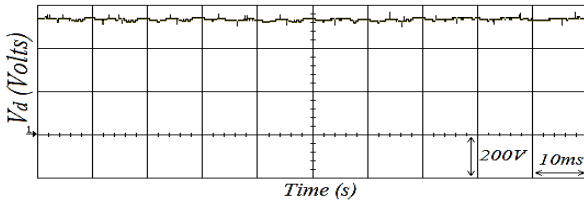


Fig. 18. Experimental input DC voltage waveform

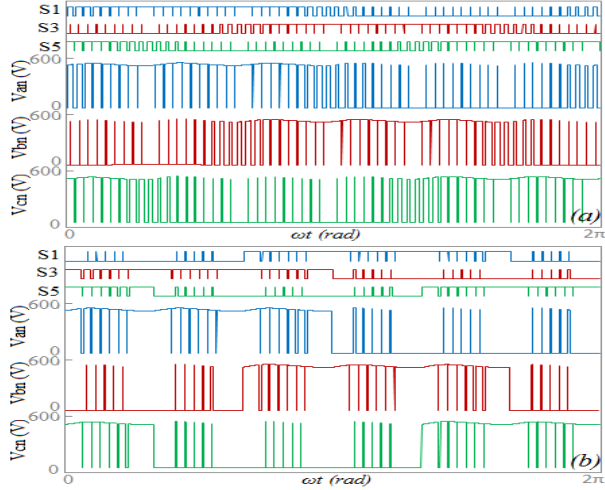


Fig. 19. Simulated switching pulses and corresponding phase voltages of the VSI for (a) linear modulation and (b) overmodulation conditions in one cycle

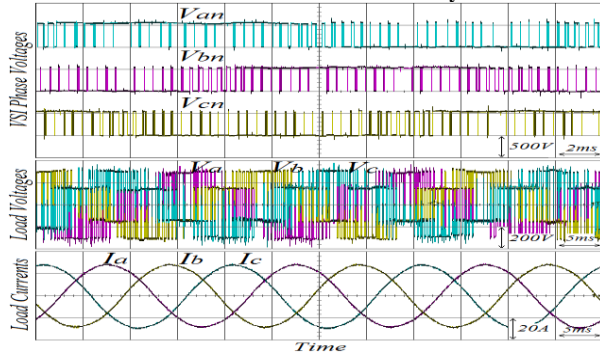


Fig. 20. Experimental phase voltages of the inverter and phase voltages and currents of the load in standard conditions

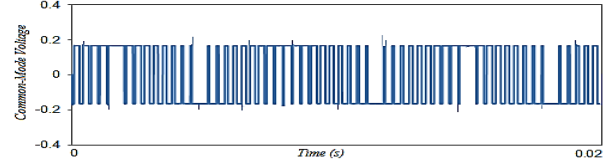


Fig. 22. The normalized common-mode voltage of the simulated VSI considering the model predictive control in the LVPWM

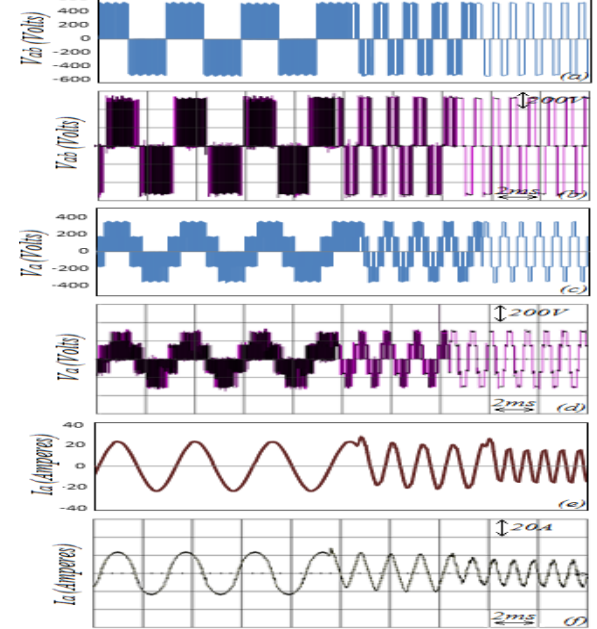


Fig. 21. Simulated and experimental results in three different conditions: (a) simulated line-line voltage, (b) experimental line-line voltage, (c) simulated phase voltage, (d) experimental phase voltage, (e) simulated phase current, (f) experimental phase current

The model predictive control strategy for reduction of the VSI common-mode voltage [21] has been implemented by the proposed LVPWM with the diagram shown in Fig. 15(b). As discussed, this method has complexity using the SVPWM and can be implemented simply by the LVPWM. Fig. 22 shows the normalized common-mode voltage of the simulated VSI considering the model predictive control strategy in the LVPWM. Compared with the inherent common-mode voltage of the inverter shown in Fig. 12, the common-mode voltage has been improved significantly by the model predictive control strategy.

8. CONCLUSIONS

A novel modulation method for voltage control of three-phase two-level voltage source inverters was proposed. The main contributions of this paper are summarized as follows:

- 1) Selection of switching vectors to synthesize the reference vectors is simple (without dependency on the number of vectors or sub-sectors). Therefore, it has lower computational overhead than SVPWM in the methods which add virtual vectors or sub-sectors to the

SVPWM diagram.

2) The proposed method conveniently selects the switching vectors in the overmodulation condition and hence results in a smooth transition from linear to overmodulation region without requiring complex computations or lookup tables.

The proposed method was applied to a simulated and laboratory-built 15-kVA VSI. The simulation and experimental results carried out in different conditions and also the harmonics analysis verify the effectiveness of the proposed algorithm.

SVPWM has computational complexity and memory requirements problems in cases of multilevel inverters. Implementation of the proposed LVPWM method for multilevel inverters is the suggestion of this paper for future researches.

REFERENCES

- [1] B. Wu, "High-power converters and ac drives", New Jersey, John Wiley & Sons, 2006.
- [2] M. Nikpayam et al., "Vector control methods for star-connected three-phase induction motor drives under the open-phase failure", *J. Oper. Autom. Power Eng.*, vol. 10, no. 2, pp. 155-164, 2022.
- [3] H. Dahmardeh, M. Ghanbari and S. M. Rakhtala, "A novel combined DTC method and SFOC system for three-phase induction machine drives with PWM switching method", *J. Oper. Autom. Power Eng.*, 2022.
- [4] I. Osman et al., "Discrete space vector modulation based model predictive torque control with no sub optimization", *IEEE Trans. Ind. Electron.*, vol. 67, no. 10, pp. 8164-74, 2019.
- [5] S. Suresh, and P. P. Rajeevan, "Virtual space vector based direct torque control schemes for induction motor drives", *IEEE Trans. Ind. Appl.*, vol. 56, no. 3, pp. 2719-2728, 2020.
- [6] Y. Wang et al., "Deadbeat model predictive torque control with discrete space vector modulation for PMSM drives", *IEEE Trans. Ind. Electron.*, vol. 64, no. 5, pp. 3537-3547, 2017.
- [7] Z. Li et al., "Modified synchronized SVPWM strategies to reduce common-mode voltage for three phase voltage source inverters at low switching frequency", *IEEE Trans. Ind. Appl.*, vol. 56, no. 5, pp. 5245-5256, 2020.
- [8] J. Sandeep, S. Ashok, and R. Ramchand, "Current error space vector based hysteresis controller for VSI fed PMSM drive", *IEEE Trans. Power Electron.*, vol. 35, no. 10, pp. 10690-99, 2020.
- [9] J. Peter et al., "Online boundary computation using sampled voltage reference for bus clamping PWM based hysteresis controlled VSI fed IM drive", *IEEE Trans. Power Electron.*, vol. 35, no. 4, pp. 3939-50, 2019.
- [10] R. Ganeshan, S. Suresh and S. S. Sivaraju, "ANFIS based multi-sector space vector PWM scheme for sensorless BLDC motor drive", *Microproc. Microsyst.*, vol. 76, pp. 1-9, 2020.
- [11] Z. Shu et al., "An efficient SVPWM algorithm with low computational overhead for three-phase inverters", *IEEE Trans. Power Electron.*, vol. 22, pp. 1797-1805, 2007.
- [12] S. D. Pablo et al., "A simpler and faster method for SVPWM implementation", *2007 Europ. Conf. Power Electron. Appl.*, 2007.
- [13] G. Vivek, and J. Biswas, "Study on hybrid SVPWM sequences for two level VSIs", *2017 IEEE Int. Conf. Ind. Tech.*, 2017.
- [14] M. A. Hannan et al., "A Random forest regression based space vector PWM inverter controller for the induction motor drive", *IEEE Trans. Ind. Electron.*, vol. 64, no. 4, pp. 2689 - 2699, 2017.
- [15] D. S. Wankhede and M. V. Aware, "A novel space vector modulation technique for two level inverter using image processing", *2017 Int. Conf. Energy, Commun., Data Analytic. Soft Comput.*, 2017.
- [16] P. Stumpf, and S. Halasz, "optimization of PWM for overmodulation region of two-level inverters", *IEEE Trans. Ind. Appl.*, vol. 54, no. 4, pp. 3393-3404, 2018.
- [17] X. Guo, M. He, Y. Yang, "Over modulation strategy of power converters: A review", *IEEE Access*, vol. 6, pp. 69528-44, 2015.
- [18] Y. Park, S. Sul, and K. Hong, "Linear over-modulation strategy for current control in photovoltaic inverter", *IEEE Trans. Ind. Appl.*, vol. 52, pp. 322-331, 2015.
- [19] H. Lee et al., "Sector based analytic overmodulation method", *IEEE Trans. Ind. Electron.*, vol. 66, no. 10, pp. 7624-32, 2019.
- [20] C. Jiang et al., "A fast model predictive control with fixed switching frequency based on virtual space vector for three-phase inverters", *2018 IEEE Int. Power Electron. Appl. Conf. Expos.*, 2018.
- [21] L. Guo et al., "Hybrid voltage vector preselection-based model predictive control for two-level voltage source inverters to reduce the common-mode voltage", *IEEE Trans. Ind. Electron.*, vol. 67, pp. 4680-91, 2020.